Phase Separation of Interpenetrating Polymer Networks Synthesized by Using an Autocatalytic Reaction

Hideyuki Nakanishi, Masahiro Satoh, Tomohisa Norisuye, and Qui Tran-Cong-Miyata*

Department of Macromolecular Science and Engineering, Graduate School of Science and Technology, Kyoto Institute of Technology, Matsugasaki, Kyoto 606-8585, Japan

Received May 29, 2006; Revised Manuscript Received September 18, 2006

ABSTRACT: Poly(*cross*-styrene)-*inter*-poly(*cross*-methyl methacrylate) interpenetrating polymer networks (IPNs) were prepared by simultaneously photo-cross-linking an anthracene-labeled polystyrene and photopolymerization of methyl methacrylate (MMA) monomer in the presence of ethylene glycol dimethacrylate (EGDMA) used as a cross-linker. The cross-linking reaction of these two polymer components is mutually independent and is drivable by irradiation with 365 nm UV light. The photopolymerization of MMA monomer exhibits an autocatalytic behavior due to the heat of polymerization and was analyzed by using a nonlinear kinetic model. As the reaction yield exceeds a certain threshold, the mixture undergoes phase separation. The time-evolution of the PMMA domains observed under a laser scanning confocal microscope follows a power law with an exponent approximately equal to unity. The domain growth was spontaneously frozen by the reactions and was terminated in a stationary bicontinuous structure whose characteristic length scales vary linearly with the kinetic parameters of the autocatalytic reaction. A general relationship for the kinetics of phase separation induced by this autocatalytic reaction was found over a large range of cross-linker concentration. Finally, the roles of the reaction autocatalysis in phase separation of polymer mixtures are discussed and compared to other cases of reaction-induced phase separation.

I. Introduction

Reaction-induced phase separation plays an important role in polymer materials science and engineering. From the practical viewpoints, this phenomenon is encountered in the fabrication of micro-optics systems such as microlens arrays using photopolymerizable acrylate or methacrylate derivatives.[1] Properties such as optical qualities of the products obtained by this fabrication method may be severely limited if phase separation occurs during the polymerization process. Therefore, information on photopolymerization-induced phase separation would provide an efficient way to control the optical properties of these materials. Fundamentally, reaction-induced phase separation belongs to a class of critical phenomena driven by the competition between reactions and phase separation through which the final morphology of the reacting mixture is determined.[2] This competition process is particularly of interest because it would provide a useful guide line to control the morphology of multiphase polymeric materials. Furthermore, the competition also renders important information on the selection process of critical fluctuations driven by antagonistic interactions.[3] In the past decade, phase separation phenomena induced by various types of chemical reactions have been theoretically and experimentally investigated for binary mixtures of small molecules and polymers. Cross-linking is the most widely utilized reaction in the thermal curing process of epoxy resins where phase separation occurs as soon as the networks fraction reaches a threshold inside the reacting mixture.[4] Phase separation induced by thermally activated reactions and polymerization was also studied.[5−7] Alternatively, coupling trans-esterification reaction to the phase separation between two polymers has also been performed in an attempt to control the morphology of multicomponent polymers.[8,9] On the other hand, to decouple the effects of heat required to activate chemical reactions from the thermodynamics of the blends, photodimerization has been efficiently utilized to control morphology of polymer blends.[10] Photoisomerization has been also demonstrated as a tool to control the mode-selection process in reaction-induced phase separation of polymer blends.[11] These experimental results verified in part the theoretical predictions of reaction−diffusion theories proposed for the roles of chemical reactions acting as a selector for critical fluctuations.[12] In particular, for reversible reactions, it was theoretically predicted that periodic structures with long wavelengths can be suppressed by the reaction, consequently leading to periodic structures similar to the morphology emerging from microphase separation of block copolymers.[13−18] These experimental results and theoretical predictions share a common view that chemical reaction plays an important role in selecting the final wavelengths of morphology for reacting polymer blends.

In polymer synthesis, it has been known for a long time that certain monomers such as methacrylate and acrylate derivatives, exhibit the autocatalytic behavior during the polymerization process. This significant behavior originates from the positive feedback driven by the successive couplings between the heat generated by the polymerization and the reaction of monomers in the surrounding initiated by this heat.[19] Though a large number of studies on the kinetics of autocatalytic reactions have been carried out, particularly with epoxy resins, in the past few decades,[20−23] the influence of the reaction autocatalysis on the phase separation induced by polymerization has not yet been intensively exploited. Many years ago, the critical phenomena associated with an autocatalytic reaction in small molecule mixtures were theoretically investigated for the first time by Huberman,[24] who showed that autocatalysis, as a nonlinear effect, can lead to the formation and selection of periodic patterns in chemical systems. On the other hand, an autocatalytic feedback on a photochemical reaction driven by critical fluctuations has been reported for a polymer blend upon irradiation.[25] Most recently, the effects of reaction autocatalysis on the kinetics of phase separation induced by a gradient of light intensity were

* To whom correspondence should be addressed. E-mail: qui@kit.ac.jp.

10.1021/ma061198w CCC: $33.50
Published on Web 11/20/2006

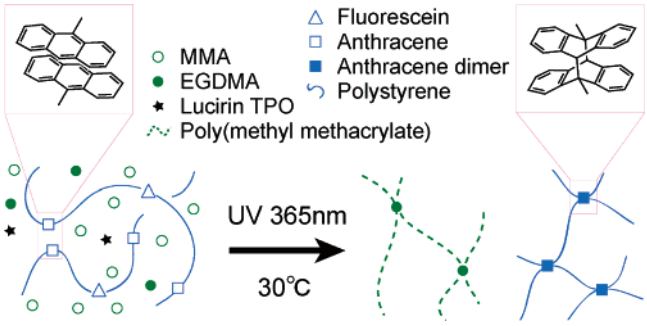

Figure 1. Schematic presentation for the chemical synthesis of the poly(*cross*-styrene)-*inter*-poly(*cross*-methyl methacrylate) IPNs used in this work.

examined by using laser scanning confocal microscope (LSCM) for a mixture of polystyrene and methyl methacrylate.[26]

In this paper, we investigated phase separation phenomena in *full*-interpenetrating polymer networks (*full*-IPNs) prepared from a homogeneous mixture of polystyrene and methyl methacrylate (MMA) monomer. First, the polymerization kinetics of the MMA component in the mixture was examined for five cross-linker concentrations. Subsequently, the kinetics of phase separation was monitored in situ under a laser scanning confocal microscope (LSCM) and the resulting morphology was analyzed by using digital image analysis techniques. From these kinetic parameters, the correlations between the autocatalytic reaction and the phase separation were investigated for these five cross-linker concentrations. The roles of the reaction autocatalysis in phase separation are finally discussed in conjunction with the resulting morphology of these IPNs.

II. Experimental Section

1. Samples. Samples used in this study are the mixtures of photocross-linkable polystyrene and methyl methacrylate monomer (MMA). Polystyrene doubly labeled with the photoreactive group anthracene and the marker fluorescein (PSAF; $M_w = 310\,000$; $M_w/M_n = 2.2$) was dissolved in MMA monomer (distilled in vacuo after removing inhibitor) and the homogeneous mixture was used as a starting material. Upon irradiation with 365 nm, anthracene moieties labeled on the PSAF chains undergo photodimerization, generating the PSAF networks. Under this irradiation condition, polymerization of MMA was initiated by Lucirin TPO, and the cross-linking reaction between PMMA chains was simultaneously induced in the presence of ethylene glycol dimethacrylate (EGDMA) which acts as a cross-linker for the PMMA component. The synthesis of this IPN is schematically described in Figure 1. To examine the effects of the cross-linker on the phase separation kinetics and the resulting morphology, the concentration of EGDMA was varied in the range 2−10 wt % with respect to the total weight of MMA monomer. Concentration of the photoinitiator Lucirin TPO was maintained at 2 wt % with respect to the MMA monomer throughout the experiments. Further details of the chemical synthesis and the characteristics of the samples used in this study were described in the previous studies.[26,27]

2. Irradiation Experiments and Observation of Morphology. Homogeneous mixtures of PSAF and MMA were irradiated under a laser scanning confocal microscope (Pascal LSM5, inverted type, Carl Zeiss). A mixture with a given composition was kept in a heating block with an insulating holder installed on the stage of the confocal microscope. The temperature of the mixture was thermostated at 30 °C with a precision of ±0.5 °C. Irradiation was performed through an optical fiber which allows UV light from a high-pressure Hg−Xe lamp (350 W, Moritex Inc., Japan) to enter perpendicularly to the sample from the top. Morphological observation was carried out in situ at 30 °C throughout this study. Irradiation intensity of the UV light at 365 nm was kept at $I = 0.01$ mW/cm^2 for all the experiments to avoid the effects of the light gradient

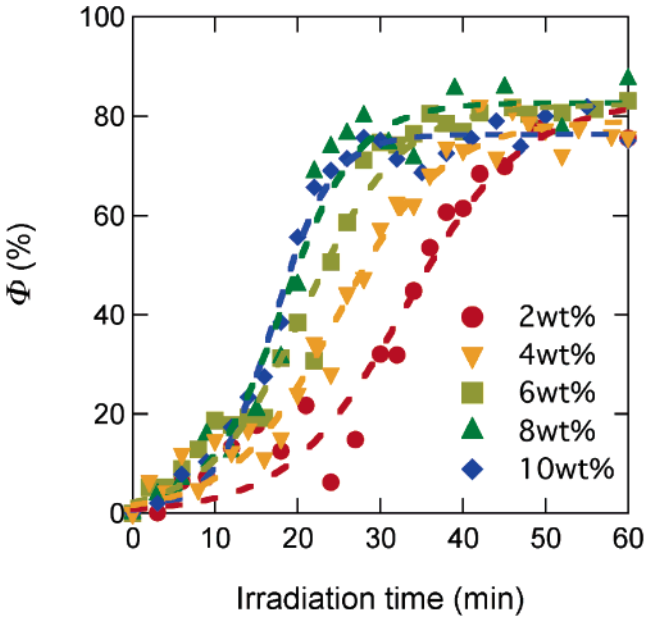

Figure 2. Kinetics of the photopolymerization of MMA monomer in a PSAF/MMA (5/95) mixture measured by FT-IR at 30 °C for various concentrations of EGDMA: (a) 2 wt %; (b) 4 wt %; (c) 6 wt %; (d) 8 wt %; (e) 10 wt %.

along the direction of illumination. It is worth noting that for higher intensity (above 0.03 mW/cm^2) the effects of the intensity gradient in the blend become significant, resulting in graded morphology as reported previously.[26] Measurements were performed with an Ar^+ ion laser (488 nm, 0.2 W). The morphology resulting from photopolymerization and photocross-link was observed with an objective lens (×40, N.A. = 0.75) and by an oil-immersed objective (×63, N.A. = 1.4) for low and high magnifications, respectively. The fluorescence images were taken with the dimensions (512 pixels × 512 pixels) and a resolution of 0.7 μm along the *Z*-direction. The procedure for the in situ monitoring of the time-evolution process of phase separation was described in details elsewhere.[26−27]

3. Morphology Analysis. For morphological analysis, the softwares ImageHyper II (Digimo Inc., Japan) and Image Visart (v.2.08, Carl Zeiss) were used respectively to analyze the particle size distribution in the 2-D images and to construct the 3-D data. The characteristic length scales of the morphology were calculated by digital image analysis. The diameters of a large number of spherical domains (between 500 and 1000) were calculated and their distribution was fitted to the following Gaussian function as described previously.[27]

$$N(D) = A \exp[-(D - \bar{D})^2/\sigma^2] \quad (1)$$

Here, $N(D)$ is the number of spherical domains with the diameter D. $\bar{D}$, the average diameter of these domains, can be obtained from the peak of this distribution function. A and σ^2 are respectively the proportional constant and the dispersion of these domain diameters. The details will be shown in the Results and Discussion below.

4. Monitoring the Reaction Kinetics. The polymerization of MMA was monitored by following the decrease in the absorption of the C═C stretching mode (1640 cm^{-1}) of the MMA monomer by FT-IR (Perkin-Elmer, model Spectrum GX) with the resolution 4 cm^{-1}. The absorption of the C═O bonds at 1720 cm^{-1} was used as an internal reference because it does not involve in the reaction. The kinetics of the polymerization of MMA was evaluated using the reaction yield Φ defined as

$$\Phi\ (\%) = \left(1 - \frac{\dfrac{(A_{C=C})_t}{(A_{C=O})_t}}{\dfrac{(A_{C=C})_{t=0}}{(A_{C=O})_{t=0}}}\right) \times 100 \quad (2)$$

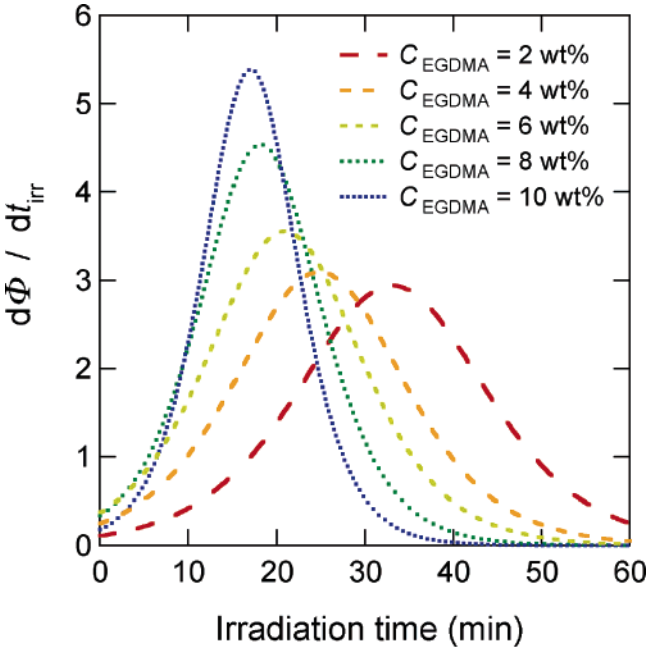

Figure 3. Irradiation-time dependence of the average reaction rate of MMA in a PSAF/MMA (5/95) mixture measured at 30 °C for various concentrations of EGDMA.

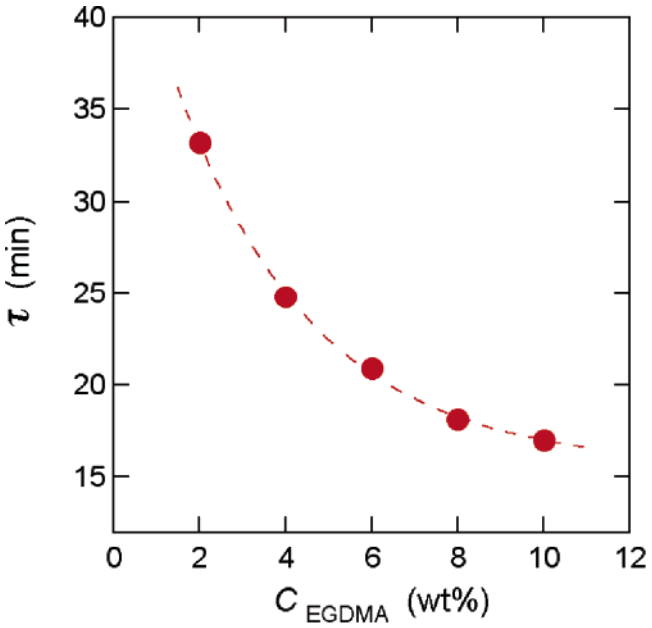

Figure 4. Dependence of the characteristic time τ on the cross-linker concentration observed for the autocatalytic reaction of MMA in a PSAF/MMA (5/95) mixture at 30 °C. The dotted line is the guide for the eyes.

where A represents the absorbance of the corresponding vibrational modes obtained from the FT-IR spectra. The reaction kinetic data were analyzed by using the software Igor Pro (Wave Metrics Inc.) on a laptop computer (La Vie G, Intel Pentium Processor 1.0 GHz, NEC). The details of the reaction kinetics studies on photocross-linked blends using FT-IR were published elsewhere.[28]

5. Determination of the Onset of Phase Separation. The fluorescence images (512 pixels × 512 pixels) of the mixture were detected with an 8-bit (gray scale) detector and were integrated to yield the total fluorescence intensity of each image observed at a given Z-coordinate. The onset of the phase separation of the mixture under irradiation with UV light was determined from the sudden decrease in the total fluorescence intensity caused by scattering at the phase domains formed upon irradiation. The intersection

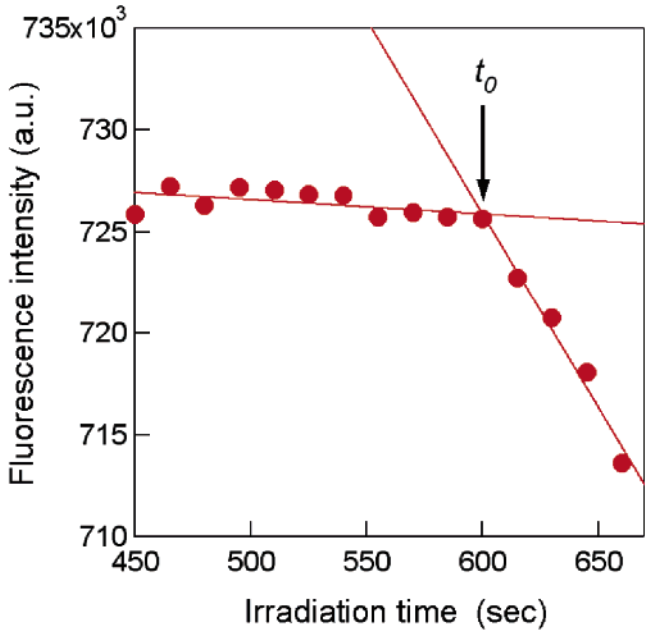

Figure 5. Determination of the onset of phase separation by using the total fluorescence intensity monotored at 30 °C for a PSAF/MMA (5/95) mixture containing 4 wt % of EGDMA.

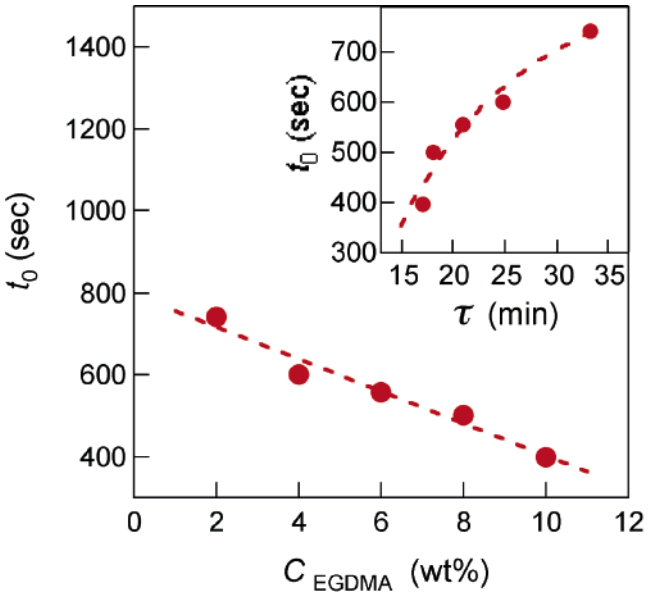

Figure 6. Dependence of the onset time t_o of phase separation on the cross-linker concentration observed for a PSAF/MMA (5/95) at 30 °C. The dotted line is a guide for the eyes.

between the two straight lines expressing the fluorescence intensity of the sample before and after this sudden change determines the cloud point of the sample.

III. Results and Discussion

1. Polymerization Kinetics of Methyl Methacrylate Monomer in the Mixture. Upon irradiation with 365 nm UV light, MMA monomer undergoes photopolymerization and photocross-link in the presence of Lucirin TPO and EGDMA. During this process, the absorbance of the C═C double bonds in MMA monomer gradually decreases with irradiation time and was in situ monitored by using FT-IR spectroscopy. The kinetic data obtained for five concentrations of the cross-linker EGDMA are illustrated in Figure 2 where the reaction yield Φ defined in eq 2 was plotted vs irradiation time (t_{irr}) for the mixtures containing 2, 4, 6, 8, and 10 wt % of EGDMA. The time-

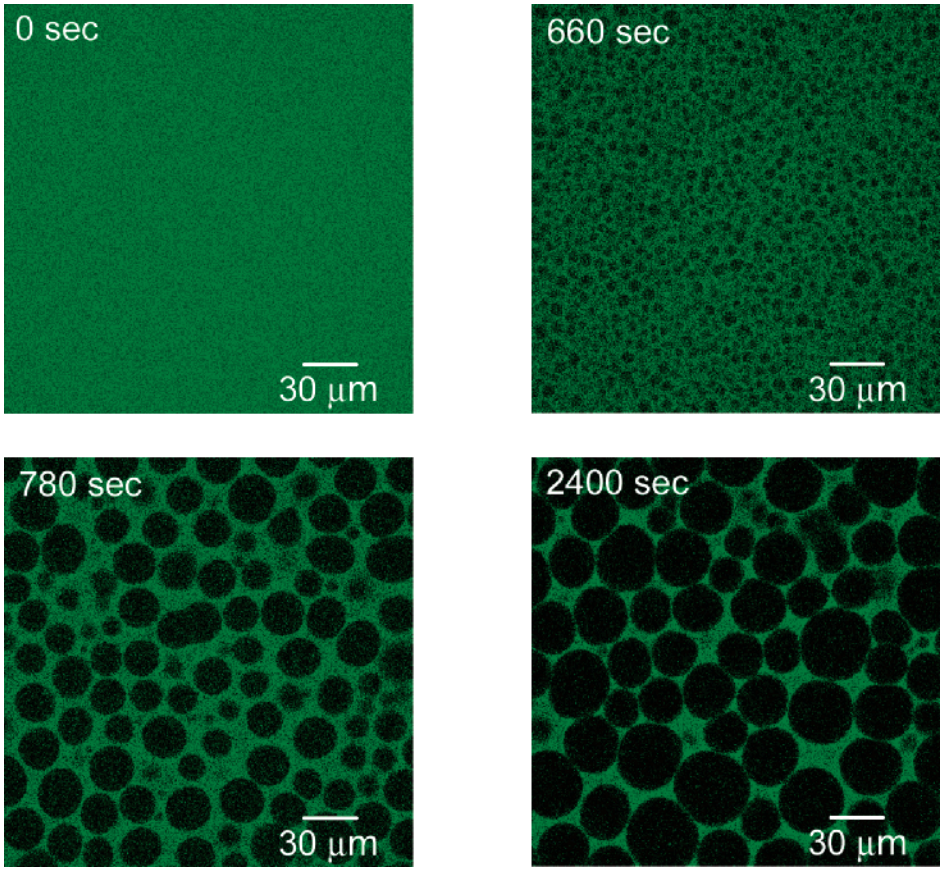

Figure 7. Time-evolution of the morphology obtained for a PSAF/MMA (5/95) mixture containing 4 wt % of EGDMA irradiated at 30 °C. The number in each image indicates irradiation time. The PMMA-rich phase appears as black domains in the morphology.

evolution of the reaction varies with the cross-linker concentration and exhibits two significant features. First, the reaction yield quickly increases with irradiation time after passing an inflection point and then approaches a limiting value of ca. 80%. The sigmoidal dependence of the reaction yield Φ on irradiation time t_{irr} was observed for all the concentrations of EGDMA. These results indicate that the polymerization of the MMA component proceeds with an autocatalytic fashion in the irradiated mixtures.[19] The inflection point on the reaction yield curve corresponds to the irradiation time at which the average rate of the polymerization reaches its maximum. To quantify this autocatalytic behavior, the kinetic data obtained with these five concentrations of EGDMA were fitted to the following empirical equation by using nonlinear least-squares with regression:[23]

$$\Phi = \Phi_f - \frac{\Phi_f}{1 + \exp[(t_{irr} - \tau)/\delta t_{irr}]} \quad (3)$$

Here, Φ and Φ_f are, respectively, the reaction yield obtained at a given irradiation time t_{irr} and the final yield of the reaction. On the other hand, τ is the characteristic irradiation time corresponding to the inflection point on the Φ (%) vs t_{irr} curve and can be calculated from the relation $(\partial^2\Phi/\partial t_{irr}^2) = 0$.

To gain some insights into the reaction kinetics, the solid curves obtained by fitting the experimental data to eq 3 were differentiated with respect to irradiation time. It is worth noting that, to increase the precision of the calculation, the data obtained by the curve fitting were used for this differentiation instead of the discrete data points obtained by experiments. The results are illustrated in Figure 3 where the average reaction rate defined by $(d\Phi/dt_{irr})$ was plotted vs the irradiation time t_{irr} for different cross-linker concentrations. As expected, the position of the peak corresponding to the characteristic time τ at which the reaction rate reaches its maximum, shifts toward the shorter irradiation time as the cross-linker concentration increases. Furthermore, the height of these peaks gradually increases with increasing concentration of the cross-linker EGDMA. This autocatalytic behavior is illustrated in Figure 4, where τ, the irradiation time required for the mean reaction rate $(d\Phi/dt_{irr})$ to reach its maximum, is plotted vs the cross-linker concentration.

Obviously, τ decreases as the concentration of EGDMA increases. This typical behavior is known as the Trommsdorff−Norrish effect in the kinetics of free radical polymerization where an increase in viscosity induced by the polymerization limits the rate of termination and consequently enhances the rate of polymerization.[19−a] Since polymerization releases heat, this additional factor further induces polymerization and complicates the kinetics.[19b,c] This result also reveals that the characteristic time τ tends to approach a limit at a high concentration of EGDMA. The quick increase in viscosity of the reacting solution with increasing the concentration of EDGMA would be responsible for this behavior.

On the other hand, the cross-linking kinetics of the PSAF was monitored through the change in the absorbance of anthracene with irradiation time using UV−visible spectroscopy. It was found that the dimerization of anthracene does not exhibit the autocatalytic behavior and the absorption of anthracene monotonically decreases with irradiation time as reported previously for other binary blends.[29] However, since the absorption spectra of anthracene partially overlap with those

of the photoinitiator Lucirin TPO, we were not able to arrive at a quantitative conclusion for the photocross-link kinetics of the PSA component.

2. Determination of the Irradiation Time Corresponding to the Onset of Phase Separation. As irradiation time increases, the fractions of PMMA and PSAF networks in the mixture increase. Phase separation occurs as soon as the yields of these components exceed a certain critical value. Since phase separation proceeds very fast in the reacting solution, the spinodal decomposition process was hardly observed under the current experimental conditions. The quantitative observation of the phase separation becomes possible under a LSCM when the viscosity of the mixture is high enough. At this stage, the reacting mixture entered the nucleation-and-growth process, allowing the in situ observation of the phase separation. For reaction-induced phase separation, there exists, in general, an induction period t_o, which is the time duration necessary for the reaction yield Φ to reach the critical threshold. To precisely analyze the phase separation kinetics, this characteristic time t_o must be determined. As described in section II-5, under a given experimental condition, the characteristic time t_o can be determined by in situ measuring the change in the integrated fluorescence intensity of the reacting mixture. As illustrated in Figure 5, the fluorescence intensity observed from a PSAF/MMA (5/95)mixture containing 4 wt % of the EGDMA cross-linker quickly drops after 600 min of irradiation using 365 nm UV light under a LSCM. The characteristic time corresponding to this transition of the fluorescence intensity is defined as t_o. The sudden decrease in the fluorescence intensity implies that the phase boundary of the mixture reaches the experimental temperature (30 °C) after 600 s of irradiation and therefore this change corresponds to the cloud point of the mixture. As expected, the induction time t_o decreases with increasing the cross-linker concentration, indicating that phase separation took place earlier in the mixtures with higher concentrations of cross-linker. The dependence of the characteristic time t_o on the EGDMA concentration is given in Figure 6, where the correlation between the time t_o for the onset of phase separation and the characteristic time τ of the reaction is illustrated in the inset. It was found that t_o strongly depends on the characteristic time τ of the autocatalytic reaction. This onset is delayed when the characteristic time τ becomes longer.

3. Observation and Morphology Imaging of Phase Separation in PSAF/MMA Mixtures. Since phase separation proceeds very fast in the mixture solution, only the nucleation-and-growth process was directly observed under the experimental conditions used in this study. Nevertheless, by using the histogram method proposed by Tanaka et al.,[30] it can be concluded that the droplet morphology shown below developed via the spinodal decomposition process. An example for such a nucleation-and-growth process is provided in Figures 7 for a PSAF/MMA (5/95) mixture containing 4 wt % of EGDMA. Initially, small nuclei with the diameter ca. 3 μm clearly appear in the irradiated mixture after 660 s of irradiation. This particular irradiation time scale is in good agreement with the cloud point data determined independently from the change in the integrated fluorescence intensity illustrated in Figure 5. As irradiation time increases, these nuclei develop into larger spherical domains and eventually attain a stationary morphology at 60 min of irradiation. Since these spherical (dark) domains are not fluorescent under excitation with 488 nm visible light, they are PMMA-rich dispersed phases. These domains are in contrast with the fluorescent (bright green) matrix containing PSAF as a main component. To examine the effects of cross-linker concentration on the morphology, irradiation experiments were carried out using mixtures with five different concentrations of EGDMA ranging from 2 to 10 wt %. It was found that these PMMA-rich domains continue growing under irradiation until the mixture reaches a stationary state caused by cross-link-induced solidification. The morphologies at the stationary state of phase separation observed in the $X-Y$ plan located in the middle of the mixture are shown, as an example, in Figure 8 for three different concentrations 2, 6, and 10% of EGDMA. It was found that under the same condition, the average diameter $\bar{D}$ of these domains decreases with increasing concentration of EGDMA, indicating the significant suppression effects of cross-linking on the time-evolution of phase separation. Furthermore, the effect of spatial constraint arising from the finite sample thickness on the growth of the PMMA-rich domains can be clearly seen in the $X-Z$ and $Y-Z$ plans of the mixture containing

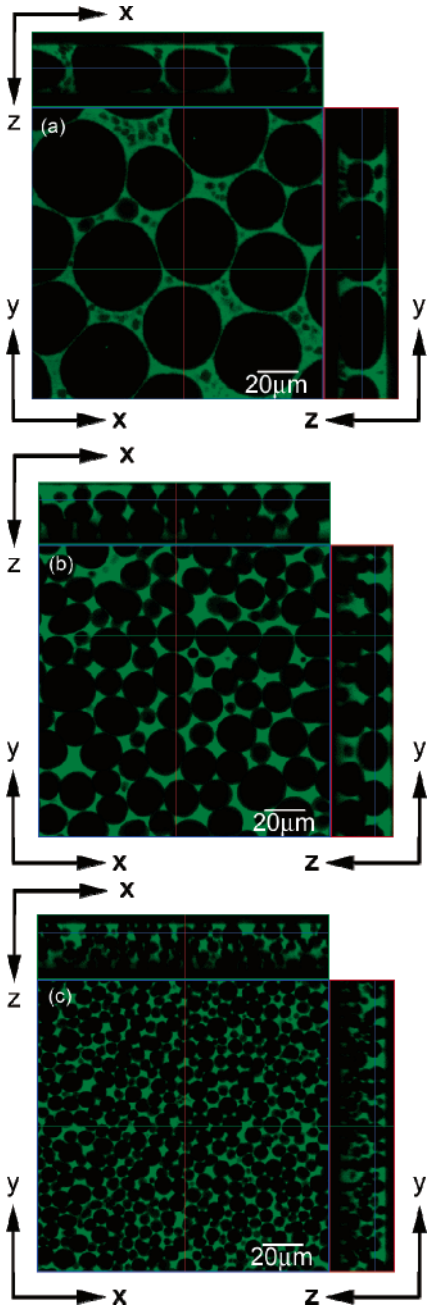

Figure 8. 3-D stationary morphology of a PSAF/MMA (5/95) mixture containing different concentrations of cross-linker observed after 60 min of irradiation at 30 °C: (a) 2 wt %; (b) 6 wt %; (c) 10 wt %.

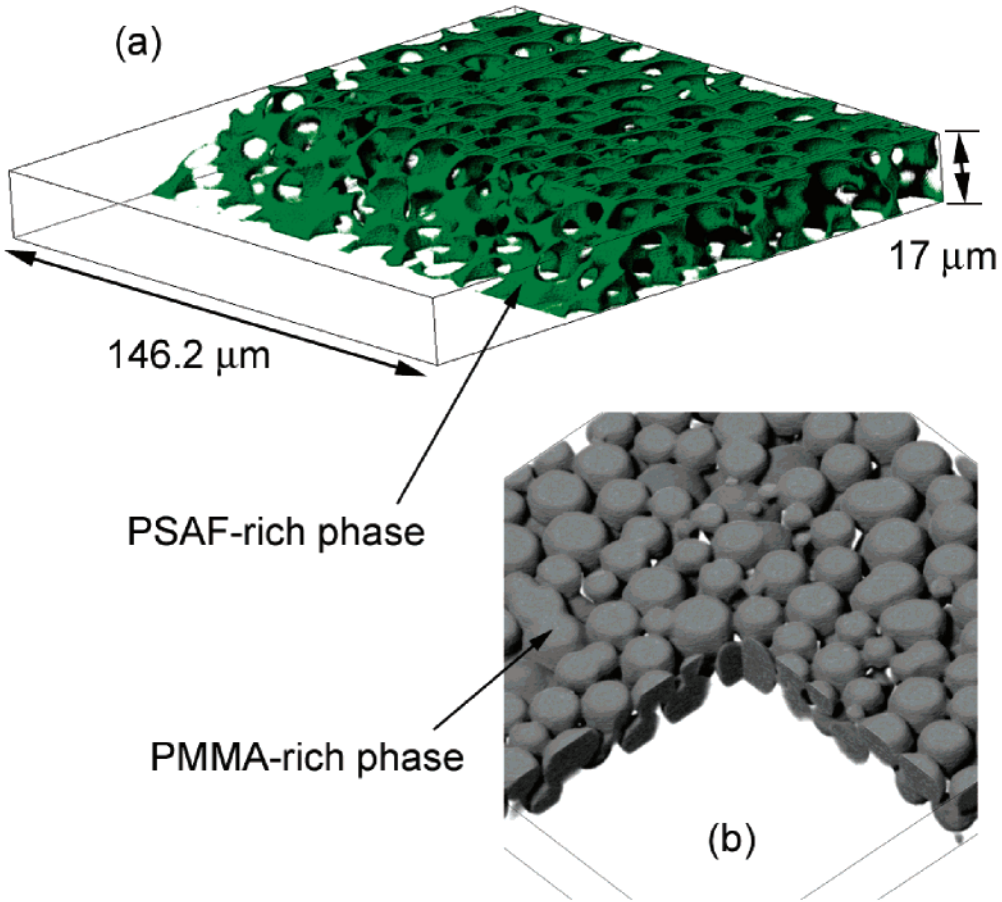

Figure 9. 3-D morphology of a PSAF/MMA (5/95) mixture obtained after 60 min of irradiation at 30 °C: (a) PSAF-rich continuous domains; (b) PMMA-rich continuous domain obtained by contrast inversion of part a. The concentration of the cross-linker EGDMA is 8 wt %.

2 wt % of EGDMA (Figure 8a). For all the cross-linker concentrations, the resulting morphology is spatially continuous as revealed by the 3-D image depicted in Figure 9. The 3-D structures were constructed from the 2-D data taken at different depths in the sample and were displayed under two different view angles. Here, the PSAF-rich (bright green) domains shown in Figure 9a form a continuous matrix covering the PMMA-rich spherical (transparent) domains. By inversing the contrast, it was found that these PMMA-rich spherical domains are also interconnected via narrow channels, forming a continuous phase of PMMA spreading through the entire IPN as illustrated in Figure 9b. The interconnecting PMMA-rich domains were probably generated by the nucleation-and-growth process followed by the combination of small nuclei with the larger ones upon coarsening due to the Ostwald ripening mechanism.[31] Subsequently, these PMMA-rich spheres develop into larger spherical domains. The number of PMMA-rich spherical domains increases with time and at the same time, the fraction of the networks also increases in these spherical domains. As the density of cross-link attains a critical value, these spherical domains can no longer be combined and start repulsing each other upon approaching. The interdiffusion of polymer chains from one droplet to another is therefore prevented by the presence of the networks, except some local areas on the surface. This conclusion is supported by the 3D morphology shown in Figure 9b where there clearly exist several "bridges" connecting different spherical domains. These interconnecting spherical domains were observed and reported previously.[27] These experimental results partially reflect the so-called viscoelastic effects in phase separation of polymer blends.[32]

It was also found from the 3-D observation that for 2 wt % of cross-linker, the diameter of the PMMA-rich domains reaches the scale comparable to the sample thickness during the phase separation process. Subsequently, these spherical PMMA-rich domains are laterally deformed into ellipsoids due to the constraint imposed by the sample thickness along the Z-direction as evidenced by Figure 8a. Eventually, these oblate domains stop growing due to the cross-link effects. The effects of this constraint on the domains growth are described below in the phase separation kinetics section.

4. Analysis of Phase Separation Kinetics Driven by an Autocatalytic Reaction. The time-evolution of the phase separation process was in situ monitored at 30 °C under an LCSM and analyzed for five concentrations 2, 4, 6, 8, and 10 wt % of the cross-linker EGDMA. To examine the phase separation kinetics, the irradiation time t_o corresponding to the onset of phase separation was measured using the procedure described in section II-5. Instead of the irradiation time t_{irr}, the time from the onset of phase separation ($t_{irr} - t_o$) was used for the analysis of the phase separation kinetics. In Figure 10, the average diameter $\bar{D}$ of the PMMA-rich domains obtained by image analysis is plotted vs the time of phase separation ($t_{irr} - t_o$). It was found that phase separation kinetics obtained for five concentrations of EGDMA shares a common behavior. In the early stage of irradiation, the scale of the PMMA-rich spherical domains quickly increases and subsequently approaches a stationary state which is independent from irradiation time. During this stage, the average diameter $\bar{D}$ of these PMMA-rich domains approximately follows the power law $\bar{D} \sim (t_{irr} - t_o)^a$ with the exponent α approximately equal to unity. This value

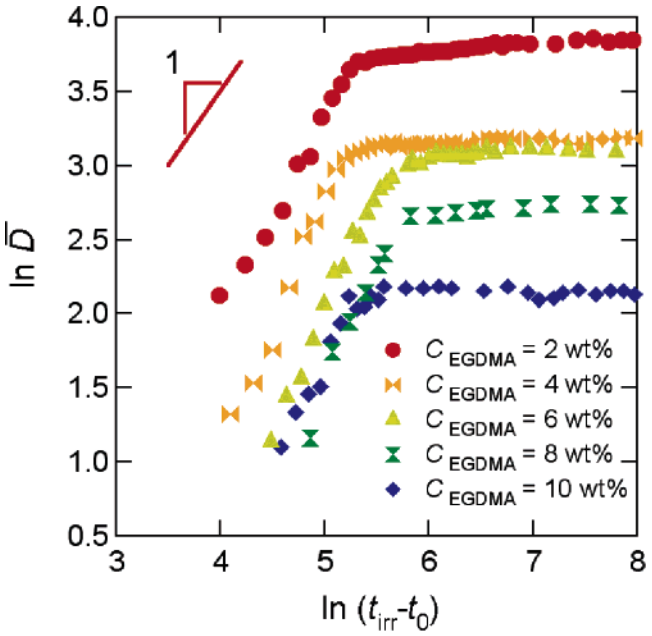

Figure 10. Irradiation-time dependence of the average diameter of the PMMA-rich domains observed at 30 °C for five PSAF/MMA (5/95) mixtures containing different concentrations of EGDMA.

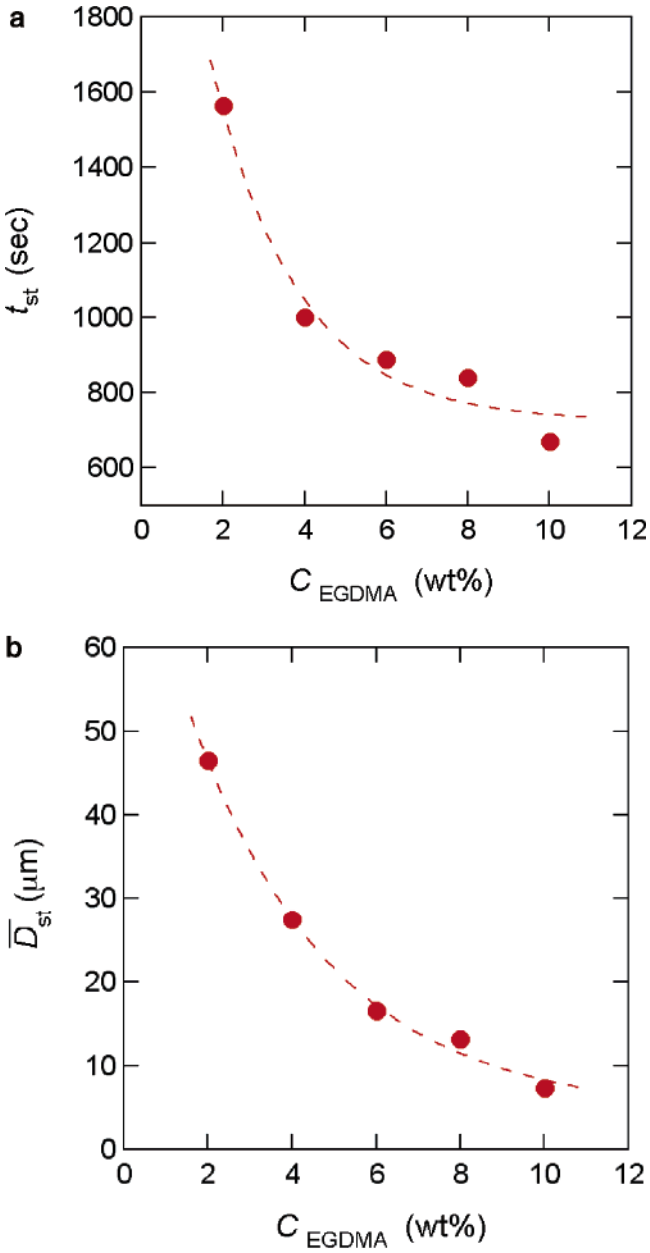

Figure 11. (a) Dependence of the characteristic time t_{st} on the cross-linker concentration obtained for a PSAF/MMA (5/95) mixtures at 30 °C. (b) Dependence of the averaged diameter of the PMMA-rich domains on the cross-linker concentration observed at 30 °C. The dotted line is a guide for the eyes.

is very close to Siggia's prediction for the effects of hydrodynamics on the phase separation kinetics.[33] Taking into account that, in general, the mixture is not at the critical composition and particularly the temperature of the mixture increases during irradiation,[34] we conclude that the exponent $\alpha = 1$ obtained in Figure 10 is probably caused by the increase in temperature accompanying with the photopolymerization, rather than by the hydrodynamic effects. Furthermore, the scale of these spherical domains gradually approached the stationary length scale $\overline{D_{st}}$ at a specific irradiation time t_{st} and eventually became unchanged with irradiation time. Both the stationary diameter $\overline{D_{st}}$ of the domains and the characteristic time scale t_{st} depend strongly on the cross-link density. Shown in Figure 11a is the dependence of t_{st} on the concentration of EGDMA. It was found that the irradiation time t_{st} required for the reacting mixture to reach the stationary state of phase separation decreases as the concentration of EGDMA increases and also becomes less sensitive in the range of high concentrations of EGDMA. This behavior can be explained by the increase in viscosity of the mixture upon increasing the EGDMA concentration. For the similar reason, the length scale $\overline{D_{st}}$ at the stationary state of phase separation also decreases with increasing the EGDMA concentration in the mixture as shown in Figure 11b. These results indicate that the time-evolution of these PMMA-rich domains was suppressed by the cross-linker as expected. Furthermore, as seen in Figure 11b, the stationary length scale $\overline{D_{st}}$ of the spherical PMMA-rich domains decreases and tends to approach a limiting value at high concentrations of EGDMA. By combining the data obtained in Figure 11, parts a and b, we can conclude that the phase separation process of the PSAF/MMA mixture can be sustained at an arbitrary stage by UV irradiation, giving polymers with various characteristic length scales.

As shown in Figure 10, the time-evolution of phase separation follows a similar fashion for various concentrations of cross-linker, suggesting the existence of a general behavior of phase separation induced by photopolymerization and photocross-link. To confirm this kinetic behavior, the normalized characteristic length scale $\bar{D}/\overline{D_{st}}$ where $\overline{D_{st}}$ is the stationary value of $\bar{D}$, was calculated and plotted vs the normalized phase separation time $(t_{irr} - t_o)/(t_{st} - t_o)$. Both $(t_{irr} - t_o)$ and $(t_{st} - t_o)$ are the irradiation time counted from t_o, the time required for the onset of phase separation. As illustrated in Figure 12, the kinetic data of phase separation obtained for all the cross-linker concentrations can be expressed by a single curve, except for the case of 2 wt % that deviates from this general behavior. It is worth noting that for a low concentration of EGDMA, the development of the PMMA-rich domains is less suppressed by the cross-link reaction and as a result their characteristic length scales can evolve and exceed the sample thickness as seen in Figure 8a. Under this particular condition, the time-evolution of the PMMA-rich domains is restricted along the direction of the sample thickness and therefore deviates from the general

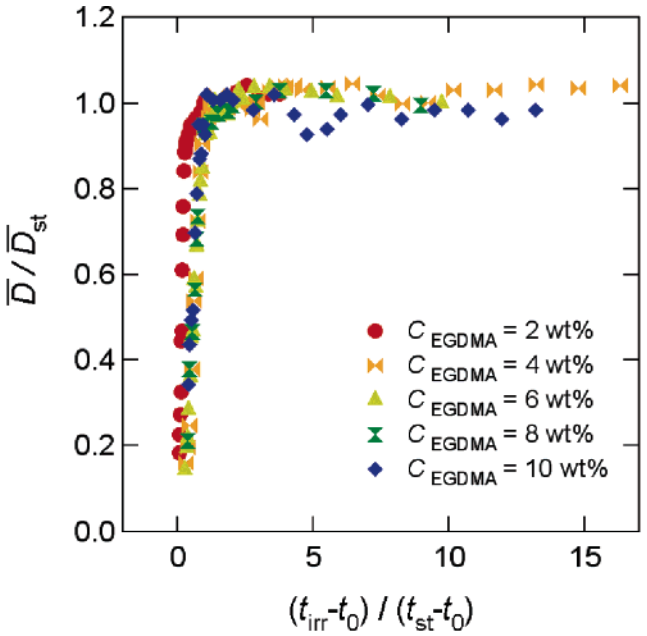

Figure 12. Reduced plot for the phase separation kinetics of a PSAF/MMA (5/95) mixture obtained at 30 °C for five different cross-linker concentrations.

relation between $\bar{D}/\overline{D_{st}}$ vs $(t_{irr} - t_o)/(t_{st} - t_o)$ compared to other cases. For higher cross-linker concentrations (4−10 wt %), all the data can be expressed by a single curve as depicted in Figure 12, revealing a general relation for the kinetics of phase separation.

On the other hand, under the experimental conditions described here, the PMMA-rich spherical domains are not monodisperse, but instead exhibit a distribution in diameter. This distribution can be calculated from the morphology taken at different irradiation time using digital image analysis as described in section II-3. As an example, the diameter distribution of these PMMA-rich spherical domains at the stationary state of phase separation observed after 60 min of irradiation was displayed in Figures 13 for five concentrations 2, 4, 6, 8, and 10 wt % of the cross-linker EGDMA. All the diameter distribution can be well fitted to the Gaussian function given in eq 1 of section II-3. From the curve fitting, the diameter distribution of these PMMA-rich domains can be calculated from the half-width at half-maximum (hwhm) Γ, which is related to the standard deviation of the Gaussian distribution via $\Gamma = (\sigma\sqrt{\ln 2}/\bar{D})$. To examine the effects of cross-linker concentration on the distribution of these spherical domains, the number N of the domains with the diameter D was normalized to the number $N_{\bar{D}}$ of domains with the average diameter $\bar{D}$ obtained from the Gaussian distribution. This normalized distribution $N/N_{\bar{D}}$ was then plotted vs the normalized length scale $D/\bar{D}$ in the reduced plot shown in Figure 14. Except for the case of 2 wt % indicated by the dotted line where the characteristic length scales of the morphology was suppressed by the sample thickness along the *Z*-direction, all the data fall on a single Gaussian curve, indicating that the morphology of the PSAF/MMA mixtures follows a general behavior as described by eq 1.

5. Correlation between Phase Separation Kinetics and Autocatalytic Reaction. For a common diffusion-controlled reaction such as cross-link in polymeric systems, the reaction rate is not a constant but usually decreases with time as the reaction proceeds because of the increase in viscosity of the medium. In contrary, for an autocatalytic reaction, the reaction rate increases with time due to the positive feedback kinetics, until it reaches a maximum at a specific time τ and subsequently decreases as the reaction proceeds further as illustrated in Figure 3. Therefore, it is expected that the kinetics of phase separation driven by an autocatalytic reaction would be different from the normal case. As shown in this study, this feature is the existence of the characteristic time scale τ in the reaction kinetics and the specific time t_{st} in the phase separation process. For a given light intensity, phase separation kinetics is determined by this characteristic time τ. Shown in Figure 15 is the correlation between the specific time τ of the reaction and the characteristic time t_{st} of the phase separation. As τ increases, the characteristic time t_{st} increases, revealing the role of the reaction in suppression of phase separation. Furthermore, the average diameter $\bar{D}_{st}$ of the PMMA-rich droplets observed at the stationary state of phase separation increases with increasing the characteristic time τ as shown in Figure 16. Several authors have theoretically proposed the correlation between the reaction rate and the stationary characteristic length scales of the morphology obtained for phase separation induced by a mean-field reaction with a constant rate k. According to these predictions, the stationary characteristic length scale ξ_∞ of the morphology would be scaled as $(1/k)^\beta$ where the exponent β is either $^1/_3$ or $^1/_4$ for phase separation under the strong or weak segregation conditions, respectively.[36,37] Phase separation induced by photoisomerization of stilbene-labeled polystyrene/poly(vinyl methyl ether) blends was previously examined, and it was found that ξ_∞ varies with the reaction rate in an opposite way with the exponent β approximately equal to 0.2 prior to the freezing of phase separation.[11a] For phase separation driven by an autocatalytic reaction, it was experimentally found that this scaling prediction does not hold. When the stationary length scale $\overline{D_{st}}$ of the PMMA-rich domains was plotted vs $1/(d\phi/dt_{irr})$ (corresponding to the inverse of the average reaction rate $\bar{k}$) on the double logarithmic scale, $\overline{D_{st}}$ increases with $1/\bar{k}$ by a power of $\beta = 2.6$, which is much larger than the value predicted by reaction−diffusion theories. This result reflects the significance of the reaction autocatalysis in the acceleration of phase separation.

An additional feature of phase separation induced by autocatalytic reaction can be observed in the two comparative experiments using a PSAF/MMA (5/95) mixture containing 4 wt % of EGDMA. In one experiment, phase separation was continuously induced by irradiation with UV light. In the other, phase separation was first induced by UV light and subsequently the UV light source was turned off after the mixture entered the unstable region of the mixture. As predicted by the Lifshitz−Slyosov−Wagner theories,[38,39] the growth exponent α approximately equal to $^1/_3$ was found for the phase separation in the dark after turning off the UV irradiation. This result is in contrast with the phase-separation kinetic data obtained by continuous UV irradiation shown in Figure 10 where the growth exponent α is approximately equal to unity. These results indicate that in the presence of UV light, the polymerization of MMA monomer is continuously promoted with additional heat of polymerization as a source of autocatalysis. It is worth noting that under the temperature conditions of this study, polymerization is almost negligible without UV light. Therefore, the heat generated by photopolymerization is a driven force for the acceleration of phase separation. As a consequence, the time-evolution of the PMMA-rich domains follows the Lifshitz−Slyosov−Wagner law for coarsening after stopping irradiation. More elaborous experiments to clarify the role of the heat

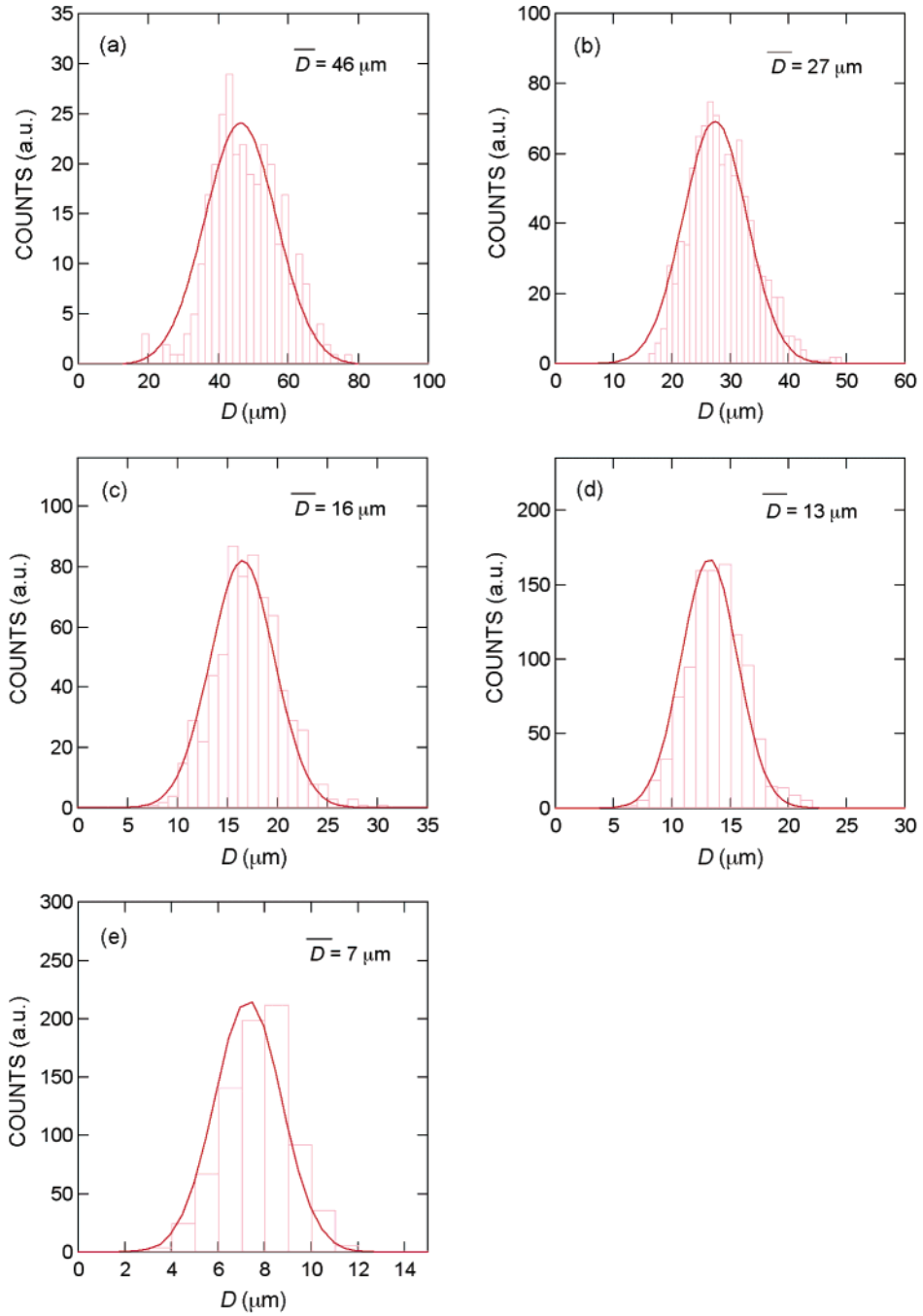

Figure 13. Distribution of the diameter of the PMMA-rich domains observed at the stationary state of a PSAF/MMA (5/95) mixture after 60 min of irradiation at 30 °C for five concentrations of EGDMA: (a) 2 wt %; (b) 4 wt %; (c) 6 wt %; (d) 8 wt % and (e) 10 wt %.

involving with the polymerization are under investigation using various light intensities, and the results will be reported later.

IV. Conclusions

We have reported the kinetics and the morphology observed during the phase separation process of an interpenetrating polymer network composed of a photocross-linkable polystyrene (PSAF) and methyl methacrylate (MMA) monomer. The following results were obtained for the coupling between the autocatalytic reaction of MMA and the phase separation of the interpenetrating polymer networks:

(1) The kinetics of photopolymerization and photo-cross-link of MMA in the presence of PSAF was monitored by FT-IR spectroscopy. It was found that the polymerization kinetics exhibits an autocatalytic behavior. This autocatalytic feedback originates from the heat generated by the photopolymerization of MMA. These results were analyzed by using a kinetic model of autocatalytic reaction, revealing the significant dependence of the reaction rate on the concentration of cross-linker.

(2) The phase separation induced by this autocatalytic reaction exhibits two-step kinetics. For the early stage of irradiation, the phase separation kinetics can be expressed by a power law with the exponent close to unity. At the later stage of irradiation, the phase separation was frozen by the cross-link reaction. The phase separation kinetics shows a general dependence on irradiation time under the experimental conditions, except for

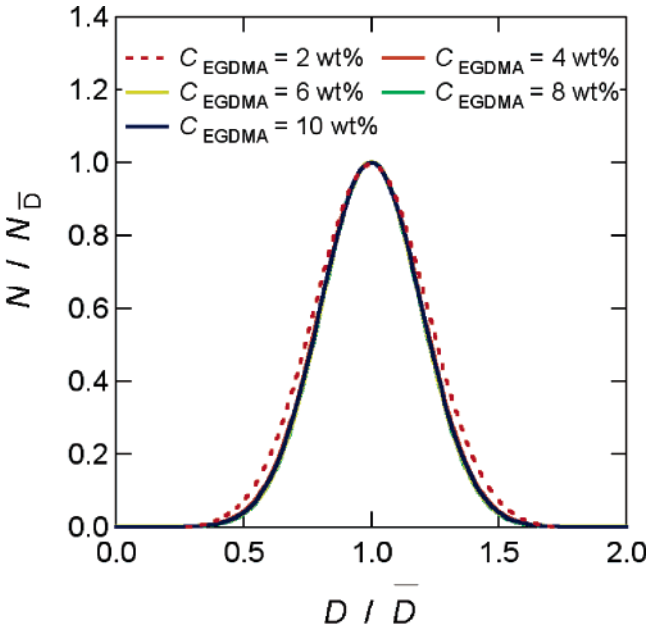

Figure 14. Reduced plot of the domain-size distribution obtained for a PSAF/MMA (5/95) mixture with five concentrations of cross-linker irradiated at 30 °C.

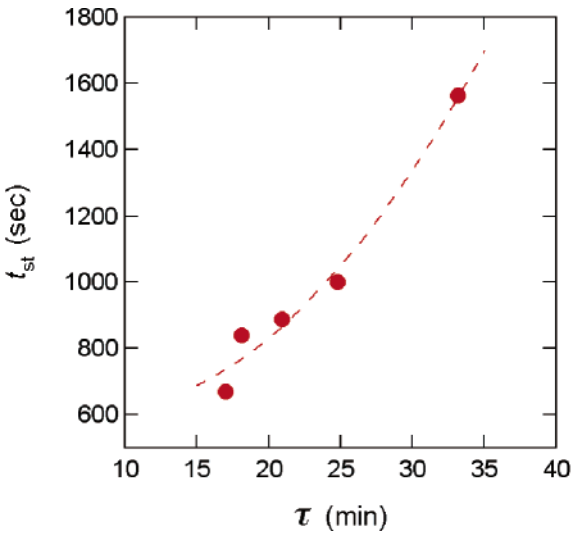

Figure 15. Correlation between the characteristic time scales of phase separation and of the autocatalytic reaction. The dotted line is a guide for the eyes.

the case of spatial constraint imposed by the sample thickness on the growth kinetics.

(3) There exists a correlation among the reaction autocatalysis and the phase separation kinetics. Compared to the conventional case induced by nonautocatalytic photochemical reactions such as photoisomerization, it was found that the phase separation proceeded faster due to the effects of the additional heat generated by photopolymerization.

Acknowledgment. This work was financially supported by the Ministry of Education, Culture, Sports, Science and Technology (MONKASHO), Japan through the Grant-in-Aid No. 16072210 on the Priority-Research-Area "Molecular Nano Dynamics". We thank Professor John A. Pojman (University of Southern Mississippi) for useful discussion on autocatalysis of polymerization.

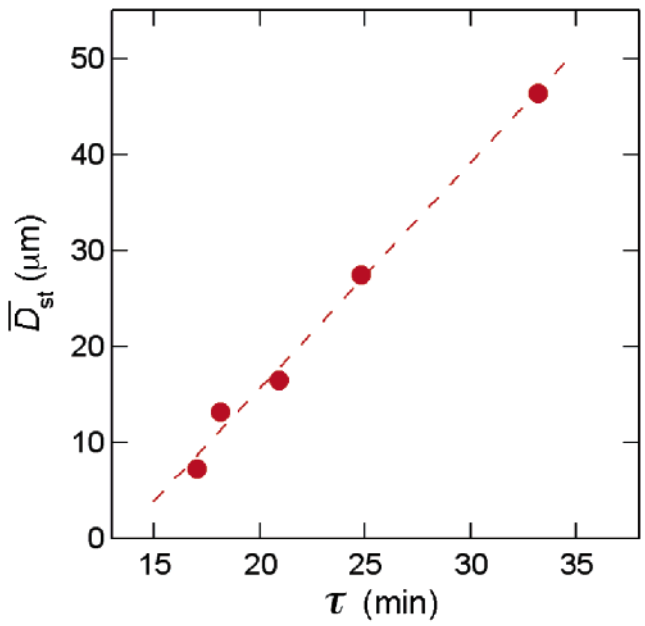

Figure 16. Correlation between the characteristic time scaleof the autocatalytic reaction and the average diameter of the PMMA-rich domains at the stationary state of the phase separation. The dotted line is a guide for the eyes.

References and Notes

(1) For example, see: Karkkainen, A. H. O.; Rantala, J. T.; Maaninen, A.; Jabbour, G. E.; Descour, M. R. *Adv. Mater.* **2002**, *14*, 535.
(2) Tran-Cong, Q.; Harada, A. *Phys. Rev. Lett.* **1996**, *76*, 1162.
(3) Seul, M.; Andelman, A. *Science* **1995**, *267*, 476.
(4) For example, see: Inoue, T. *Prog. Polym. Sci.* **1995**, *20*, 119.
(5) Okada, M.; Sakaguchi, T. *Macromolecules* **1995**, *28*, 1795; ibid. **1999**, *32*, 4154.
(6) (a) Gan, W.; Yu, Y.; Wang, M.; Tao, Q.; Li, S. *Macromolecules* **2003**, *36*, 7746. (b) Yu, Y.; Wang, M.; Gan, W.; Tao Q.; Li, S. *J. Phys. Chem. B* **2004**, *108*, 6208.
(7) Henderson, I. C.; Clarke, N. *J. Chem. Phys.* **2005**, *123*, 144903.
(8) Tanaka, H.; Suzuki, T.; Hayashi, T.; Nishi, T. *Macromolecules* **1992**, *25*, 4453.
(9) Porter, R. S.; Wang, L.-H. *Polymer* **1992**, *33*, 2019.
(10) (a) Tran-Cong, Q.; Nagaki, T.; Nakagawa, T.; Yano, O.; Soen, T. *Macromolecules* **1989**, *22*, 2720. (b) Tamai, T.; Imagawa, A.; Tran-Cong, Q. *Macromolecules* **1994**, *27*, 7486. (c) Imagawa, A.; Tran-Cong, Q. *Macromolecules* **1995**, *28*, 8388. (d) Harada, A.; Tran-Cong, Q. *Macromolecules* **1997**, *30*, 1643.
(11) (a) Ohta, T.; Urakawa, O.; Tran-Cong, Q. *Macromolecules* **1998**, *31*, 6845. (b) Nishioka, H.; Kida, K.; Yano, O.; Tran-Cong, Q. *Macromolecules* **2000**, *33*, 4301.
(12) Tran-Cong, Q.; Kawai, J.; Endoh, K. *Chaos* **1999**, *9*, 298.
(13) Glotzer, S. C.; Di Marzio, E. A.; Muthukumar, M. *Phys. Rev. Lett.* **1995**, *74*, 2034.
(14) (a) Verdasca, J.; Borckmans, P.; Dewel, G. *Phys. Rev. E* **1995**, *52*, 4616. (b) Verdasca, J.; Borckmans, P.; Dewel, G. *Phys. Rev. E* **1997**, *55*, 4828.
(15) Carati, D.; Lefever, R. *Phys. Rev. E* **1997**, *56*, 3127.
(16) Motoyama, M.; Ohta, T. *J. Phys. Soc. Jpn.*. **1997**, *66*, 2715.
(17) (a) Hildebrand, M.; Mikhailov, A. S.; Ertl, G. *Phys. Rev. E* **1998**, *58*, 5483. (b) For review, see: Mikhailov, A. S.; Hildebrand, M.; Ertl, G. Nonequilibrium Nanostructures in Condensed Reactive Systems. In *Coherent Structures in Classical Systems. Proceedings of the XVII Sitges Conference*; Reguera, D., Bonilla, L. L., Rubí, J. M., Eds.; Lecture Notes in Physics 567; Springer: New York, 2001; pp 252−269.
(18) (a) Huo, Y.; Zhang, H.; Yang, Y. *Macromol. Theory Simul.* **2004**, *13*, 280. (b) Huo, Y.; Jiang, X.; Zhang, H.; Yang, Y, *J. Chem. Phys.* **2003**, *118*, 9830.
(19) See, for example: (a) Billmayer, F. W., Jr. *Textbook of Polymer Science*; John Wiley & Sons: New York, 3nd ed.; 1984; Chapter 3. (b) Epstein, I. R.; Pojman, J. A. *An Introduction to Nonlinear Chemical Dynamics;* Oxford University Press: London; 1998; Chapter 11. (c) *Nonlinear Dynamics in Polymeric Systems*; Pojman, J. A., Tran-Cong-Miyata, Q., Eds.; ACS Symposium Series 869; American Chemical Society: Washington DC; 2004.

(20) Kamal, M. R.; Sourour, S. *Polym. Eng. Sci.* **1973**, *13*, 59.
(21) Ryan, M. E.; Dutta, A. *Polymer* **1979**, *20*, 203.
(22) Kenny, J. M. *J. Appl. Polym. Sci.* **1994**, *51*, 761.
(23) Younes, M.; Wartewig, S.; Lellinger, D.; Strehmel, B.; Strehmel, V. *Polymer* **1994**, *35*, 5269.
(24) Huberman, B. A. *J. Chem. Phys.* **1976**, *65*, 2013.
(25) Tran-Cong, Q.; Harada, A.; Kataoka, K.; Ohta, T.; Urakawa, O. *Phys. Rev. E* **1997**, *55*, R6340.
(26) Nakanishi, H.; Namikawa, N.; Norisuye, T.; Tran-Cong-Miyata, Q. *Soft Matter* **2006**, *2*, 149.
(27) Nakanishi, H.; Satoh, M.; Norisuye, T.; Tran-Cong-Miyata, Q. *Macromolecules* **2004**, *37*, 8495.
(28) Ishino, S.; Nakanishi, H.; Norisuye, T.; Awatsuji, Y.; Q. Tran-Cong-Miyata *Macromol. Rapid Commun.* **2006**, *27*, 758.
(29) Kataoka, K.; Harada, A.; Tamai, T.; Tran-Cong, Q. *J. Polym. Sci., Polym. Phys.* **1998**, *36*, 455.
(30) Tanaka, H.; Yokokawa, T.; Abe, H.; Hayashi, T.; Nishi, T. *Phys. Rev. Lett.* **1990**, *65*, 3136. The time-evolution of the fluorescence intensity histogram monitored under irradiation changes from a single peak to bimodal at 600 min, while the fluorescence intensity of these two peaks gradually increases before approaching a stationary state. These results indicate that the droplet morphology shown in Figure 7 has developed via the spinodal decomposition process.
(31) Ratke, L.; Voorhees, P. W. *Growth and Coarsening: Ostwald Ripening in Material Processing*; Springer-Verlag: New York, 2002.
(32) Tanaka, H. *J. Phys.: Condens. Matter* **2000**, *12*, R207−R264.
(33) Siggia, E. D. *Phys. Rev. A* **1979**, *20*, 595.
(34) Temperature of the mixtures was directly measured during the photopolymerization process by using two methods: a homemade mini-thermocouple sunk into the mixture under irradiation and a calibrated infrared sensor (Keyence Inc., Japan). The same results were obtained with these two methods: the temperature of the mixture increases from 30 to 33 °C during 60 min of irradiation.
(35) Tang, X.; Zhang, L.; Wang, T.; Yu, Y.; Gan, W.; Li, S. *Macromol. Rapid Commun.* **2004**, *25*, 1419.
(36) Glotzer, S. C.; Coniglio, A. *Phys. Rev. E* **1994**, *50*, 4241.
(37) Christensen, J. J.; Elder, K.; Fogedby, H. C. *Phys. Rev. E* **1996**, *54*, R2212.
(38) Lifshitz, I. M.; Slyosov, V. V. *J. Phys. Chem. Solids* **1961**, *19*, 35.
(39) Wagner, C. Z. *Z. Elektrochem.* **1961**, *65*, 581.

MA061198W